Soils and Foundations 2015;55(4):866–880

HOSTED BY

ELSEVIER

CrossMark

The Japanese Geotechnical Society

Soils and Foundations

www.sciencedirect.com
journal homepage: www.elsevier.com/locate/sandf

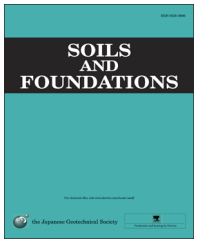

Reliability analysis of strip footing considering spatially variable undrained shear strength that linearly increases with depth

Dian-Qing Li[a,*], Xiao-Hui Qi[a], Zi-Jun Cao[a], Xiao-Song Tang[a], Wei Zhou[a], Kok-Kwang Phoon[b], Chuang-Bing Zhou[c]

[a]*State Key Laboratory of Water Resources and Hydropower Engineering Science, Wuhan University, 8 Donghu South Road, Wuhan 430072, PR China*
[b]*Department of Civil and Environmental Engineering, National University of Singapore, Blk E1A, 07-03, 1 Engineering Drive 2, Singapore 117576, Singapore*
[c]*School of Civil Engineering and Architecture, Nanchang University, Nanchang 330031, PR China*

Received 13 October 2014; received in revised form 4 February 2015; accepted 19 April 2015
Available online 21 July 2015

Abstract

This paper aims to investigate the reliability of strip footing in the presence of spatially variable undrained shear strength that linearly increases with depth. A non-stationary random field is used to model the spatially varying undrained shear strength. A strip footing example is presented to investigate the effect of spatially variable undrained shear strength on the performance of strip footing. The results indicate that the mean bearing capacity for spatially variable undrained shear strength is smaller than that obtained from a deterministic analysis. Both the mean and standard deviation of bearing capacity increase with increasing autocorrelation length. Ignoring the trend of undrained shear strength linearly increasing with depth will significantly overestimate the probability of failure of the strip footing. A factor of safety significantly below 3.0 may be used for designing strip footings if the trend of undrained shear strength linearly increasing with depth is considered properly.

Key words: Strip footing; Bearing capacity; Spatial variability; Random field; Reliability analysis

1. Introduction

In geotechnical engineering, both the deterministic approach and probabilistic approach have been used to evaluate the bearing capacity of a shallow foundation. Soil parameters generally vary spatially in both the horizontal and vertical directions (Li et al., 2011, 2015c; Cao and Wang, 2014; Jiang et al., 2015). Due to this nature, the probabilistic approach to evaluate the bearing capacity considering spatial variability in soil parameters has received more attention recently. A number of studies investigated the effect of spatial variability in soil properties on bearing capacity of shallow foundations (e.g. Fenton et al., 2008; Popescu et al., 2005; Kasama et al., 2012; Soubra and Mao, 2012; Teixeira et al., 2012; Wang and Cao, 2013).

The assessment of the stability of shallow foundations highly depends on the selection of a proper random field model for describing the spatial variability in soil properties. In the literature (e.g. Ching and Phoon, 2013a,b; Cho and Park, 2010; Griffiths et al., 2006, 2011; Jiang et al., 2014; Le, 2014; Lloret-Cabot et al., 2014; Low et al., 2007; Phoon et al., 2003; Zhu and Zhang, 2013; Zhu et al., 2013), the stationary random field model has been widely used to describe the spatial variability of soil parameters. In this model, a spatially variable parameter is customarily decomposed into a trend function and

*Corresponding author. Tel.: +86 27 6877 2496; fax: +86 27 6877 4295.
E-mail address: dianqing@whu.edu.cn (D.-Q. Li).
Peer review under responsibility of The Japanese Geotechnical Society.

http://dx.doi.org/10.1016/j.sandf.2015.06.017

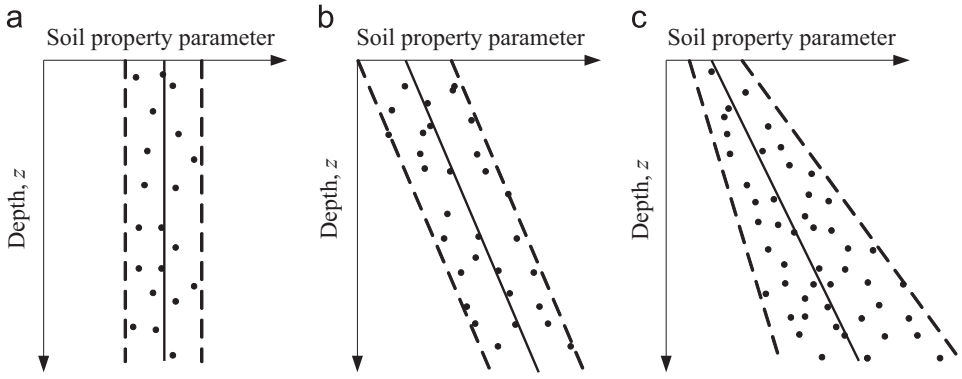

Fig. 1. Different types of spatial variability of soil property.

a fluctuating component (Phoon and Kulhawy, 1999). Note that the stationarity refers to as a weak or second-order stationarity. In other words, the mean and standard deviation of soil parameter do not vary with depth, and the covariance between the fluctuating components at two different depths is a function merely of their separation distance instead of the absolute position. Some data from in situ tests, however, reveal that the stationarity does not always characterize the spatial variability of soil property (e.g. Asaoka and A-Grivas, 1982; Haldar and Sivakumar Babu, 2009; Kulatilake and Um, 2003; Lumb, 1966; Li et al., 2014; Sivakumar Babu et al., 2006). Therefore, it is necessary to investigate the effect of spatially variable soil properties on shallow foundation reliability using a non-stationary random field model.

In view of the non-stationary characteristic underlying the spatial variability of soil properties, a number of researchers have paid attention to the non-stationary random field of spatially variable soil parameters(e.g. Kulatilake and Um, 2003; Sivakumar Babu et al., 2006; Srivastava and Sivakumar Babu, 2009). For example, Kulatilake and Um (2003) evaluated the variance and correlation distance of cone tip resistance (q_c) using two different random field models, namely one random field model with a constant trend function (stationary) and the other random field model with a linear trend function (non-stationary). They pointed out that the stationary random field model may produce misleading correlation distance. Sivakumar Babu et al. (2006) modeled the spatial variability of q_c using a non-stationary random field with a quadratic trend function, which was further used for the reliability analysis of a shallow foundation. Srivastava and Sivakumar Babu (2009) adopted a non-stationary random field with a linear trend function to describe the spatial variability of q_c associated with shallow foundation and slope stability problems. However, the non-stationary random field of undrained shear strength (s_u) where both the mean and standard deviation of s_u linearly increase with depth as reported in Lumb (1966) has not been investigated. Additionally, it is recognized that the coefficient of variation (COV) of s_u also varies with depth in the non-stationary random field of s_u. For convenience, however, a COV of s_u at the depth of influence zone is often adopted to represent the overall COV of s_u in geotechnical reliability problems (e.g. Sivakumar Babu et al., 2006; Srivastava and Sivakumar Babu, 2009). The resultant errors caused by this simplification are not clear. To validate this simplification, it is necessary to compare the reliability results obtained from a constant COV and a non-constant COV underlying the spatially variable s_u.

Table 1
Statistics of soil strength properties with depth z (modified from Lumb (1966)).

Soil	Property	Mean (μ)	Standard deviation (σ)	COV (%)
Marine clay in Hong Kong	s_u (kPa)	$1.04z+1.89$	$0.19z+0.35$	18.4
London clay	s_u (kPa)	$22.1z$	$3.58z$	16.2

This paper aims to investigate the reliability of strip footing in the presence of spatially variable undrained shear strength that linearly increases with depth. A non-stationary random field where both the mean and standard deviation of s_u linearly increase with depth is used to model the spatial variability of s_u, which is discretized by Karhunen–Loeve (KL) expansion (e.g. Phoon et al., 2002). Monte Carlo simulations are carried out to evaluate the statistics of bearing capacity and reliability of strip footing. For comparison, the corresponding results obtained from the stationary random field of s_u are also provided. A strip footing example is presented to investigate the effect of spatial variability on the statistics of bearing capacity and the reliability of strip footing.

2. Spatial variability of undrained shear strength

Soil is a complex engineering material that has been formed by a combination of various processes, such as geologic, environmental, and physical–chemical processes (Tang et al., 2013, 2015). Soil properties in situ exhibit spatial variability due to the effect of these natural processes. After examining the statistical properties of London Clay and four types of soils in Hong Kong, Lumb (1966) divided the spatial variability in soil property into the following three types (see Fig. 1): (a) mean and standard deviation of soil parameter constant with depth; (b) mean of soil parameter linearly increasing with depth while standard deviation of soil parameter constant with depth; (c) both mean and standard deviation of soil parameter

linearly increasing with depth. Types (a) and (b) usually appear in soil properties such as friction angle, cohesion, compression index et al (Lumb, 1966). The reliability analysis of geotechnical engineering problems involving these two types of spatial variability is well documented in the literature (e.g. Ching and Phoon, 2013a,b; Srivastava and Sivakumar Babu, 2009). The spatial variability of type (c), however, is only confined to the undrained shear strength parameter (see Table 1). The effect of this kind of spatial variability on the performance of geotechnical engineering systems has not been well studied. Hence, this paper will mainly focus on the spatial variability of undrained shear strength belonging to type (c). Since type (a), namely stationary spatial variability, is widely used in geotechnical reliability problems, the corresponding results for type (a) are also provided for comparison. For brevity, the spatial variability with mean and standard deviation linearly increasing with depth is referred to as non-stationary spatial variability in the context of this study.

Although the soil data in Lumb (1966) (see Table 1) indicates that non-stationary spatial variability does exist in reality, the mechanism behind this non-stationarity is still unclear. Hence, the trend of undrained shear strength with depth is investigated using an empirical relation between undrained shear strength, current effective vertical stress (σ'_{vo}), and the overconsolidation ratio (OCR) of clay soil, namely Eq. (1). This relation is usually used to predict the undrained shear strength for slightly plastic and medium plastic soils (Kulhawy and Mayne, 1990). As shown in Eq. (1), the effective vertical stress and OCR are indispensable when deriving the value of s_u. Thus, realistic values of effective vertical stress are first calculated according to unsaturated soil mechanics. Second, OCR data from different sites are collected. On these bases, rational undrained shear strength profiles are obtained using Eq. (1).

$$s_u/\sigma'_{vo} = (0.23 \pm 0.04)\mathrm{OCR}^{0.8} \tag{1}$$

2.1. Effective vertical stress

It is well recognized that effective vertical stress is highly influenced by water pressure. For overconsolidated clay soils, a ground water table is commonly located at a shallow depth below the ground surface. Soil suction or negative pore water pressure always exists in the unsaturated zone above the ground water table. It is necessary to consider the water pressure using knowledge of unsaturated soil mechanics to obtain a realistic effective stress. In unsaturated soils, the effective stress is not the difference between total stress and pore water pressure, but rather the difference between the total stress and some function of negative pore water pressure or soil suction. The general form of effective stress, σ', for variably saturated soils (including both saturated and unsaturated soils) is given by Lu et al. (2010)

$$\sigma' = (\sigma - u_a) - \sigma^s \tag{2}$$

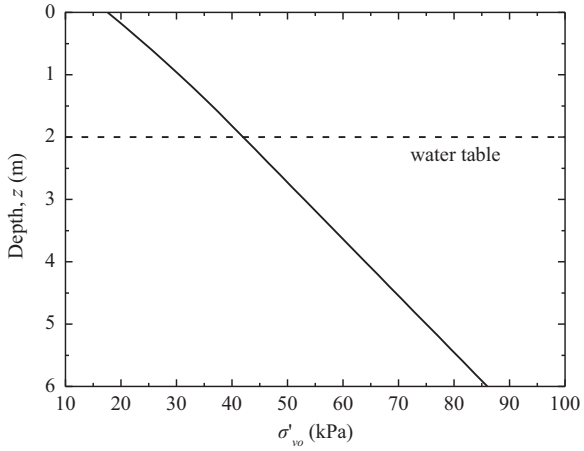

Fig. 2. Effective vertical stress varying with depth for a typical clay soil considering soil suction.

where σ is the total stress, u_a is the pore air pressure, σ^s is suction stress which is given by

$$\sigma^s = -\frac{\theta-\theta_r}{\theta_s-\theta_r}(u_a-u_w) \tag{3}$$

where θ is the volumetric water content, θ_r is the residual volumetric water content, θ_s is the saturated volumetric water content, and u_w is pore water pressure. Lu et al. (2010) show that suction stress can relate solely with u_a-u_w, as follows:

$$\begin{cases} \sigma^s = -(u_a-u_w) & \text{if } u_a-u_w \le 0 \\ \sigma^s = -\frac{(u_a-u_w)}{(1+[\alpha(u_a-u_w)]^n)^{(n-1)/n}} & \text{if } u_a-u_w > 0 \end{cases} \tag{4}$$

where α and n are two parameters in a commonly used soil water characteristic curve(SWCC) model (van Genuchten, 1980). Note that the SWCC is an equation that describes the relationship between the water content and matric suction.

As a component of the effective stress, the effective vertical stress, σ'_{vo}, can be simply derived from Eqs. (2) to (4) as

$$\begin{cases} \sigma'_{vo} = \sigma_v - u_w & \text{if } u_a-u_w \le 0 \\ \sigma'_{vo} = (\sigma_v-u_a) + \frac{(u_a-u_w)}{(1+[\alpha(u_a-u_w)]^n)^{(n-1)/n}} & \text{if } u_a-u_w > 0 \end{cases} \tag{5}$$

where σ_v is the total vertical stress, which can be expressed as $\sigma_v=\gamma_{\text{total}}\, z$, in which γ_{total} denotes the total unit weight of the soil and z denotes the depth below the ground surface. The distribution of u_w with depth is quite complex, depending on the boundary conditions of seepage on the ground surface. One possible solution is the hydrostatic suction distribution, i.e.

$$u_w = \gamma_w(z-z_{wt}) \tag{6}$$

where γ_w is the unit weight of water, z_{wt} is the depth of water table. This solution is a reasonable estimation of the in situ pore water pressure as no rainfall, evaporation, or vegetable cover exist (Collins and Znidarcic, 2004). Based on Eqs. (5)–(6), the effective vertical stress can be easily obtained. For example, for a typical overconsolidated clay with γ_{total}=21 kN/m^3, γ_w=10 kN/m^3, z_{wt}=2 m, α=0.03 kPa^{-1}, n=1.5, the effective vertical stress varying with depth is plotted in Fig. 2. As shown in Fig. 2, the σ'_{vo} approximately linearly increases with depth from the ground surface.

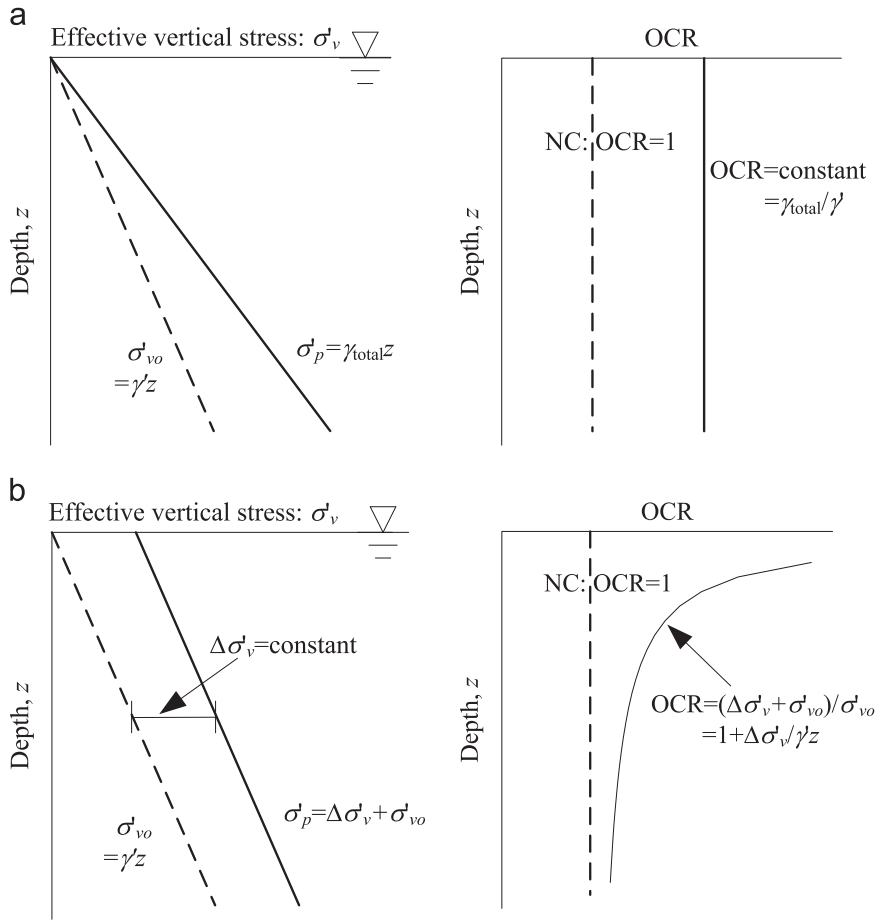

Fig. 3. Profiles of stress history and OCR caused by different mechanics. (a) Groundwater fluctuation (b) Erosion, glacial action or excavation.

2.2. OCR data

As shown in Eq. (1), an OCR profile is needed to obtain an empirical s_u curve. The overconsolidation ratio is defined as

$$\mathrm{OCR} = \sigma'_p/\sigma'_{vo}. \tag{7}$$

where σ'_p is the effective vertical preconsolidation stress, which is the maximum vertical effective stress experienced by a point in a soil mass in the past. The in situ OCR profile is quite complex, depending on the combined effect of many environmental factors. Possible factors include erosion, glaciations, removal of overburden, fluctuation of the groundwater table and desiccation due to surface drying or capillary flow. For example, (a) if a normally-consolidated (NC) deposit is subject to groundwater lowering, such as during a drought condition, and then the water table returns, a resulting profile of constant OCR $=\gamma_{total}/\gamma'$ with depth occurs (see Fig. 3(a)). (b) In another case, if an overburden pressure($\Delta\sigma'_v$) is removed from a normally-consolidated deposit due to natural erosion or glacial activity, the associated OCR is inversely proportional to depth, as shown in Fig. 3(b). Details of the theoretical OCR profiles caused by different mechanics can be found in Chen and Mayne (1994).

Although the theoretical OCR profiles in Fig. 3 provide a basis to understand the mechanics of how OCR develops, they may be too simple to consider the combined effect of various factors. Hence, OCR data from different sites (Chen and Mayne, 1994) are collected to reflect the true in situ situation of stress history (see Fig. 4). The OCR data are fitted to a curve using the function form of

$$\mathrm{OCR} = l + m/(z+p) \tag{8}$$

where l, m and p are curve fitting parameters. This functional form is specifically selected because it represents the real mechanics of consolidation. The constant part, namely l, is the OCR induced by the water table fluctuation (see Fig. 3(a)), while the reciprocal function part, $m/(z+p)$, represents the OCR trend caused by erosion or removal of overburden pressure. As shown in Fig. 4, all the curves can well capture the trend of OCR with depth. Besides, all the coefficients of determination (R^2) for the fitting have values larger than 0.78, indicating a good fit. Hence, these curves are further used to estimate the trend of undrained shear strength with depth using Eq. (1).

2.3. Undrained shear strength varying with depth

With the effective vertical stress and OCR curve been decided, the trend of s_u with depth can be easily estimated using Eq. (1). Similar to Section 2.1, parameters of $\gamma_{total}=21$

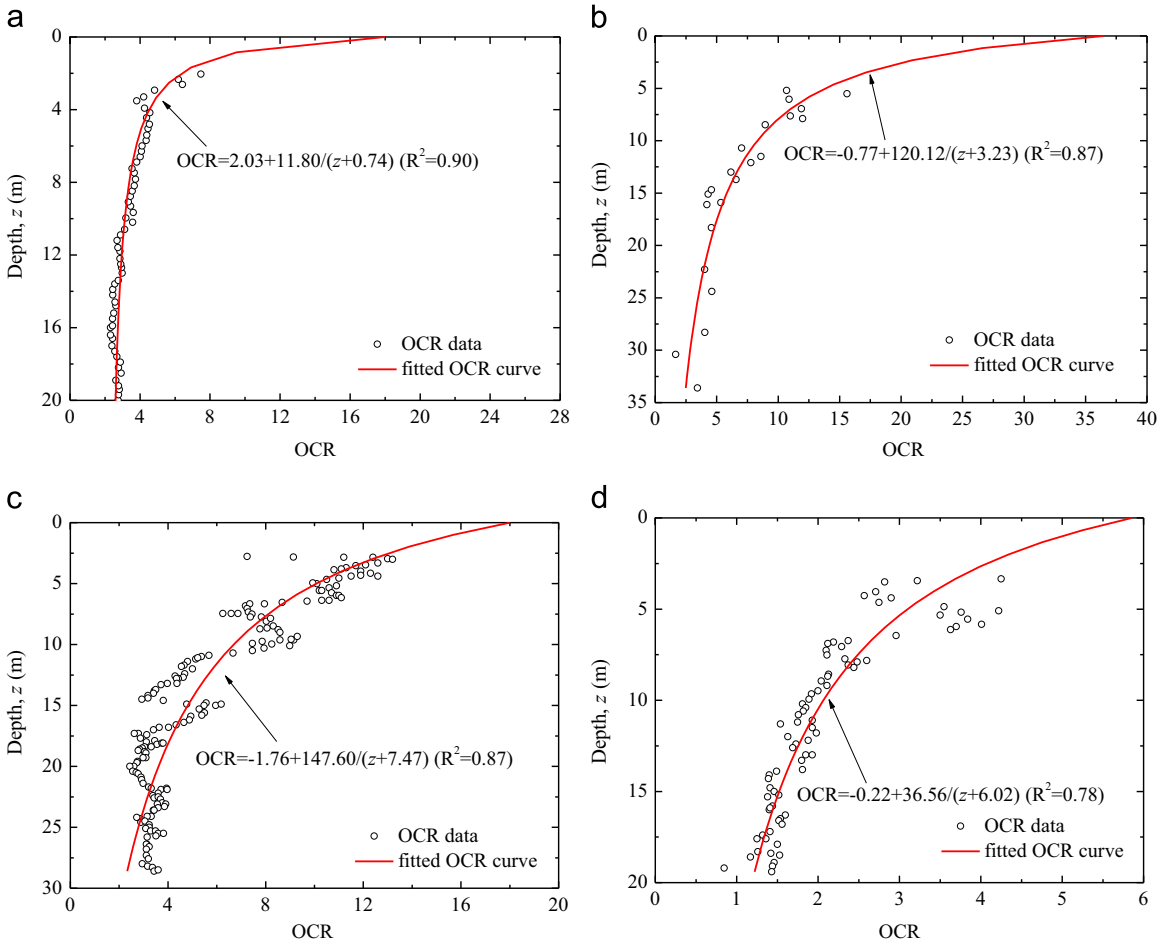

Fig. 4. Collected OCR data from various sites. (a) Port Huron, USA(b) Baton Rouge, USA (c) Kringalik Plateau, Canada (d) Ontario, Canada.

kN/m^3, $\gamma_w = 10$ kN/m^3, $z_{wt} = 2$ m, $\alpha = 0.03$ kPa^{-1}, $n = 1.5$ for a typical clay soil are adopted. These parameters are used to obtain the effective vertical stress. The fitted OCR curves in Fig. 4 are adopted to provide OCR profiles. The lower and upper bound of s_u can be estimated from Eq. (1), i.e. lower bound $= 0.19\text{OCR}^{0.8}\sigma'_{vo}$ and upper bound $= 0.27\text{OCR}^{0.8}\sigma'_{vo}$. Fig. 5 shows the variation of these lower and upper bounds with depth for different sites. As shown in Fig. 5, all the bounds of s_u display an approximately linear trend with depth. Simple linear trends falling within these bounds can be reasonably selected (i.e. the solid straight lines in Fig. 5). Note that for normally consolidated soils with a water table at the ground surface, the OCR $= 1$ and $\sigma'_{vo} = \gamma' z$. For this case, the lower bound and upper bound of s_u can be expressed by two straight lines, i.e. lower bound $= 0.19\sigma'_{vo} = 0.19\gamma' z$ and upper bound $= 0.27\sigma'_{vo} = 0.27\gamma' z$. Asaoka and A-Grivas (1982) also pointed out that s_u can increase linearly with depth from a non-zero value for overconsolidated soils, and from zero for normal consolidated soils. This conclusion is consistent with the simple model adopted in this study.

It must be noted that a nearly constant trend of undrained shear strength also exists in reality. This always occurs in unsaturated, stiffed clayey soils (e.g. Shibuya and Tanaka, 1996), where the suction in shallow depths may significantly improve the strength of soil (see Eqs. (1) and (5)). It might be risky to adopt a constant trend model when the undrained shear strength actually displays a linearly increasing trend with depth. It is the engineer's responsibility to discern the real trend and choose the right model (stationary or non-stationary) for reliability analysis.

3. Simulation of spatial variability of undrained shear strength

As discussed in Section 2.1, the undrained shear strength is likely to linearly increase with depth as follows:

$$s_u = a\sigma'_{vo} + b = a\gamma' z + b \tag{9}$$

where a is the increasing rate of the undrained shear strength with depth; b is the value of the undrained shear strength at the ground surface ($z = 0$). Values of a and b can be estimated using the linear regression approach (e.g. Vanmarcke, 2010). Note that b takes the value of 0 for normal consolidated soils according to the discussion in Section 2.3. This study adopts a linear trend that falls between the lower and upper bounds of the undrained shear strength as shown in Fig. 5(c). In addition, the COV of the unit weight of soils is below 0.1 (Phoon and Kulhawy, 1999). Following Wu et al (2012), it can be treated

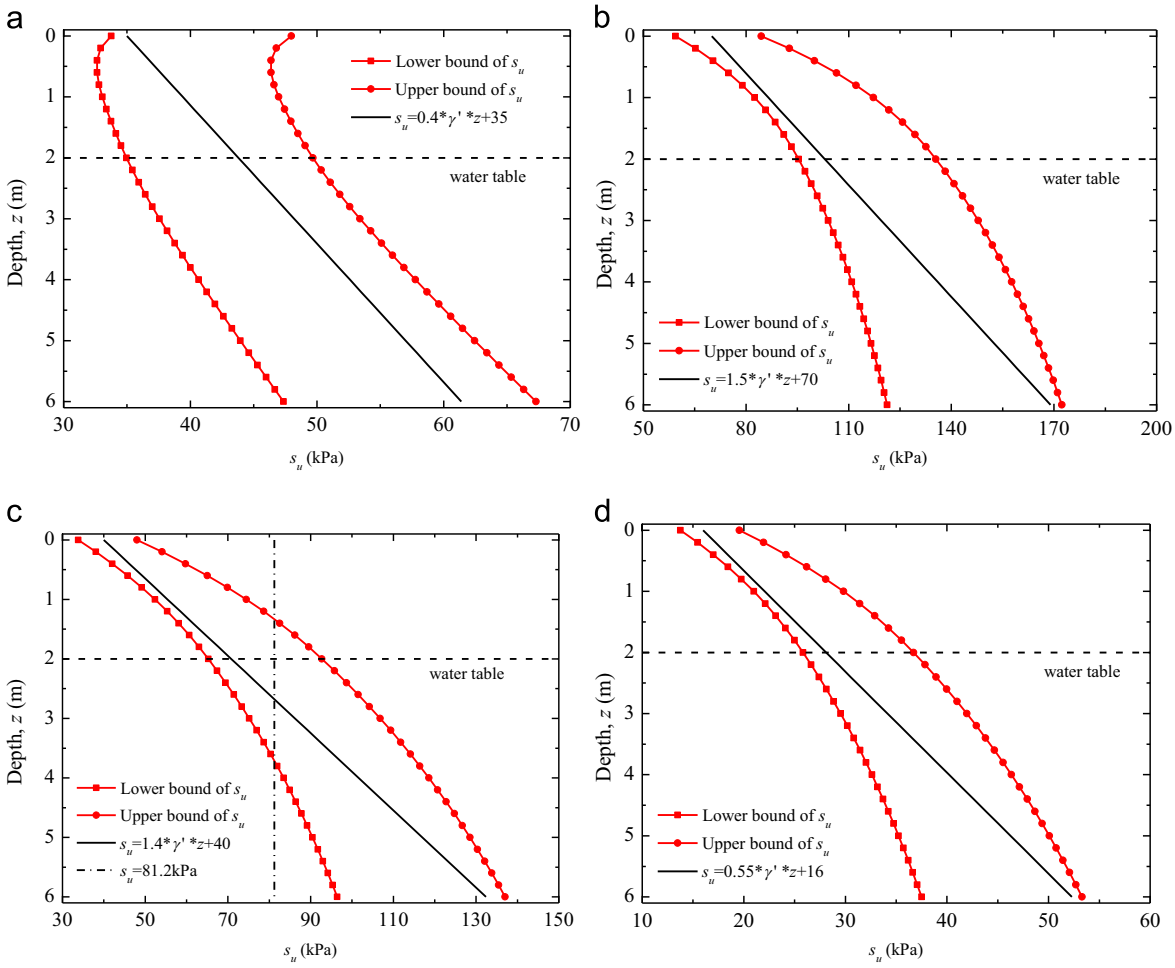

Fig. 5. Estimated s_u varying with depth. (a) Port Huron, USA(b) Baton Rouge, USA (c) Kringalik Plateau, Canada (d) Ontario, Canada.

as a lognormally distributed random variable. The parameter b is considered to be deterministic for simplicity. The spatial variability of s_u is modeled by treating the parameter a as a stationary random field (Luo et al., 2012; Wu et al., 2012). In this way, the statistics of s_u are derived as

$$\begin{cases} t_{su}(z) = \mu_{a\gamma'} z + b \\ \sigma_{su}(z) = \sigma_{a\gamma'} z \\ \mathrm{COV}_{su}(z) = \dfrac{\mu_{a\gamma'} z + b}{\sigma_{a\gamma'} z} \end{cases} \tag{10}$$

in which $t_{su}(z)$, $\sigma_{su}(z)$ and COV_{su} are the mean, standard deviation and COV of s_u, respectively; $\mu_{a\gamma'}$ and $\sigma_{a\gamma'}$ are the mean and standard deviation of $a^*\gamma'$, respectively. It is evident that both the mean and standard deviation of s_u in Eq. (10) linearly increase with depth, which is consistent with the statistical data for s_u in Table 1.

As for the distribution of a, Lacasse and Nadim (1996) suggested that both normal and lognormal distributions can be approximately used to describe a. To avoid negative values, the marginal distribution of a is considered to be a lognormal distribution. Hence, the mean and standard deviation of $a^*\gamma'$ in Eq. (10) can be simply calculated by treating $\ln(a^*\gamma') = \ln(a) + \ln(\gamma')$ to be a normally distributed random variable, where $\ln(a^*\gamma')$, $\ln(a)$ and $\ln(\gamma')$ are the natural logarithm of $a^*\gamma'$, a and γ', respectively. Details of the calculation are omitted here. The mean and standard deviation of the natural logarithm of a are respectively given by

$$\begin{cases} \lambda_{\ln a} = \ln(\mu_a) - 0.5\ln(1+\mathrm{COV}_a{}^2) \\ \xi_{\ln a} = \sqrt{\ln(1+\mathrm{COV}_a{}^2)} \end{cases} \tag{11}$$

in which $\lambda_{\ln a}$ and $\xi_{\ln a}$ are the mean and standard deviation of the natural logarithm of a, respectively.

The autocorrelation function is an important parameter for characterizing a random field. For simplicity and convenience (Li et al., 2015a,b), a common squared exponential function is adopted as an autocorrelation function of $\ln(a)$, i.e.

$$\rho_{\ln a}(x_1, z_1; x_2, z_2) = \exp\left(-\left(\frac{x_1 - x_2}{l_x}\right)^2 - \left(\frac{z_1 - z_2}{l_z}\right)^2\right) \tag{12}$$

where $\rho_{\ln a}$ is the correlation coefficient between $\ln(a(x_1, z_1))$ and $\ln(a(x_2, z_2))$; (x_1, z_1) and (x_2, z_2) are coordinates of two arbitrary points within the area in which the random field is discretized; l_x and l_z are the correlation lengths of $\ln(a)$ in the horizontal and vertical (depth) directions, respectively.

Unlike the case where the mean and standard deviation of undrained shear strength increase with depth, the random

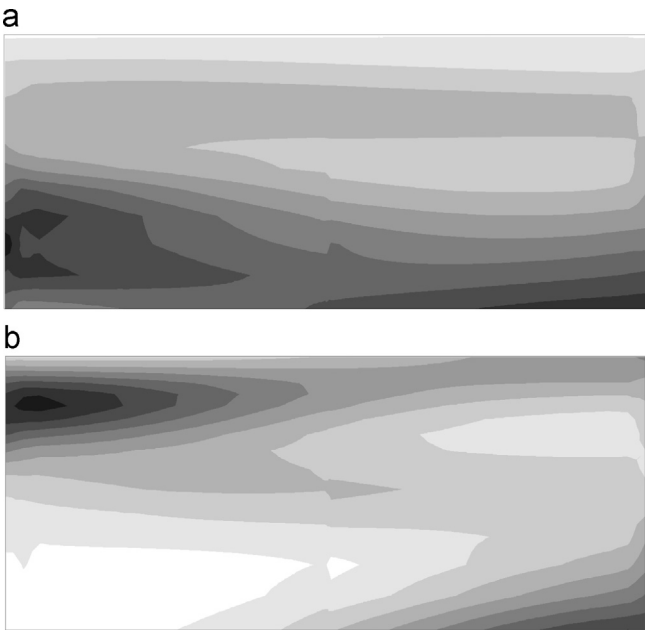

Fig. 6. Typical realizations of random field of undrained shear strength. (a) Non-stationary random field of s_u (μ_a=1.4, COV$_a$=0.50, b=40kPa, $\mu_{\gamma'}$=11 kN/m^3, COV$_{\gamma'}$=0.10, l_x=10m, l_z=1m), (b) Stationary random field of s_u (μ_{su}=86.2kPa, COV$_{su}$=0.27, l_x=10m, l_z=1m).

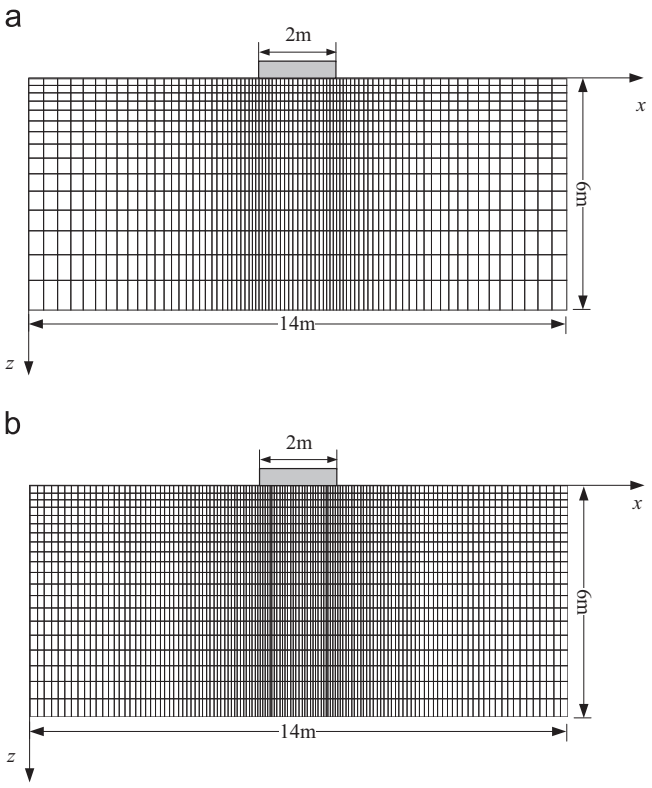

Fig. 7. Flac3d model used for bearing capacity analysis. (a) mesh scheme 1, (b) mesh scheme 2.

field for the undrained shear strength constant with depth is stationary. Thus, its simulation is similar with that for a as discussed earlier. The mean and standard deviation of the natural logarithm of s_u are respectively given by Li et al. (2014)

$$\begin{cases} \lambda_{\ln\, su} = \ln(\mu_{su}) - 0.5 \cdot \ln(1+\mathrm{COV}_{su}^{\,2}) \\ \xi_{\ln\, su} = \sqrt{\ln(1+\mathrm{COV}_{su}^{\,2})} \end{cases} \tag{13}$$

in which $\lambda_{\ln su}$ and $\xi_{\ln su}$ are the mean and standard deviation of the natural logarithm of s_u, respectively. Note that both μ_{su} and COV$_{su}$ in Eq. (13) are constants.

For computational efficiency, the KL expansion is used to discretize the random field of undrained shear strength. More details on the KL expansion can be referred to Cho and Park (2010) and Phoon et al. (2002). Similar to Cho and Park (2010), an efficient Latin hypercube sampling technique is adopted to generate the Gaussian random variables used for the KL expansion. The Latin hypercube sampling is a stratified sampling designed to ensure that the upper or lower ends of the distributions for the simulated random variables are well represented. The Monte Carlo simulation time can be greatly saved by using this sampling technique. Applying the KL expansion, one realization of non-stationary random field for undrained shear strength is plotted in Fig. 6(a). For comparison, the corresponding realization of stationary random field for undrained shear strength is plotted in Fig. 6(b). In these two figures, light colors represent low values of s_u while dark colors represent high values of s_u. In Fig. 6(a), as s_u increases with depth, s_u at the bottom of the strip footing takes high values. In the case of s_u constant with depth, s_u at the bottom of the strip footing may take low values (Fig. 6(b)). This weak zone with low values of s_u is distributed irregularly.

4. Illustrative example

In this section, a plane strain finite difference analysis is performed to calculate the bearing capacity (q_u) of a rigid strip footing founded on a clay soil with spatially variable undrained shear strength parameter. The finite difference analysis is carried out with the help of Flac3d which is a widely-used commercial software in geotechnical engineering. The spatial variability in soil properties can be effectively considered in Flac3d by assigning different values to different finite difference elements (Cho and Park, 2010). First, the results obtained from deterministic analysis using Flac3d are validated by both analytical and numerical solutions in the literature. Second, probabilistic analyses are carried out to investigate the effect of spatially variable undrained shear strength that linearly increases with depth on the reliability of strip footing.

4.1. Deterministic analysis of strip footing

Consider a rigid strip footing resting on an overconsolidated undrained clay soil, as shown in Fig. 7. Following Cho and Park (2010), a two-dimensional plane strain model is adopted to calculate the bearing capacity of strip footing and elastic-perfectly plastic behavior of the soil material with Mohr–Coulomb yield criterion is assumed. For a typical overconsolidated clay, the total unit weight of the soil is set to 21 kN/m^3.

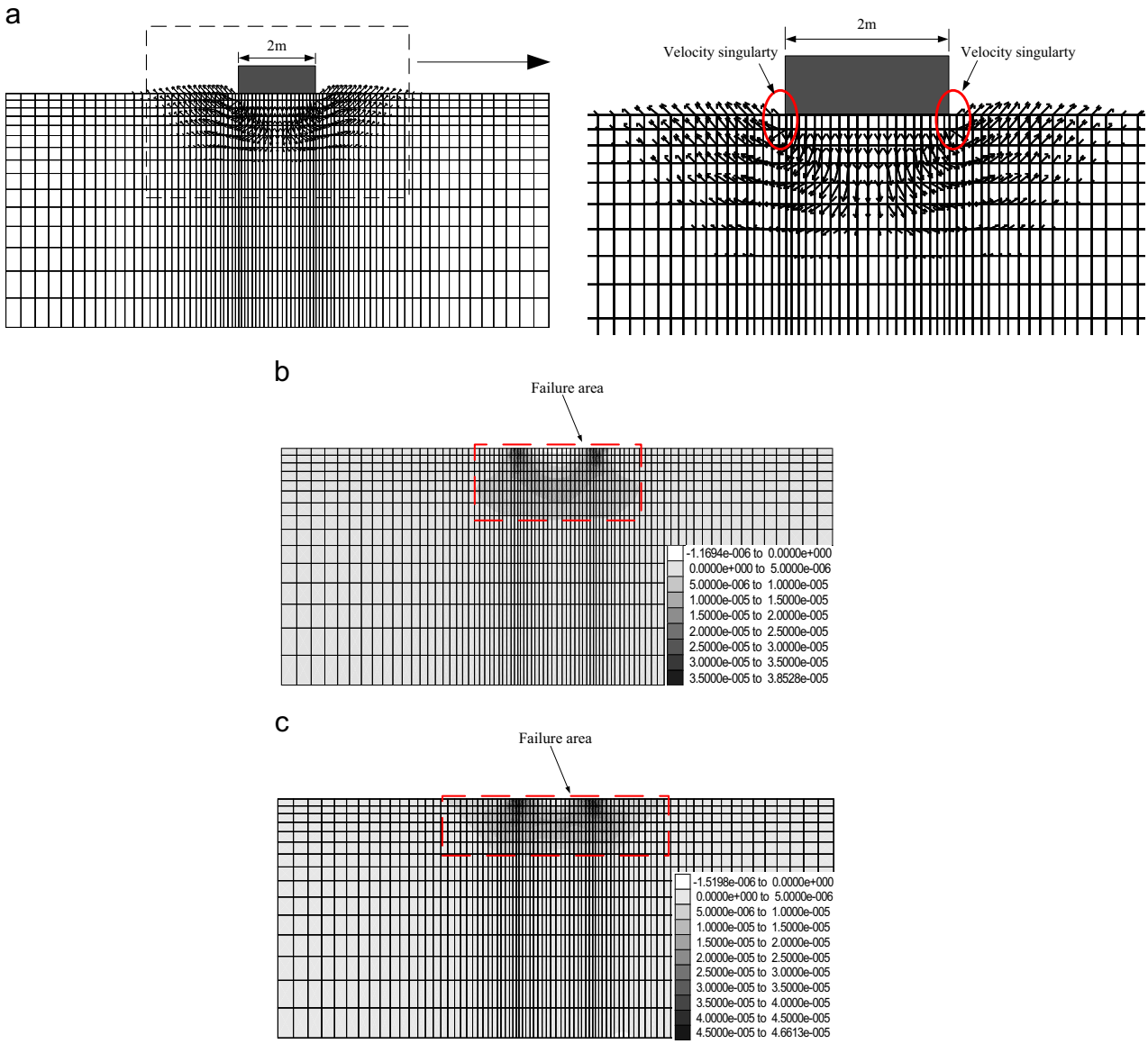

Fig. 8. The maximum shear strain rate at the plastic steady state for constant and linearly increasing s_u, respectively. (a) Velocity vector for s_u constant with depth, (b) Maximum shear strain rate for s_u constant with depth, (c) Maximum shear strain rate for s_u linearly increasing with depth.

The strip footing is rough, with a width of 2 m. The finite difference model is 14 m in width and 6 m in depth. A mesh scheme consisting of 1200 finite difference elements is adopted for the bearing capacity analysis (see Fig. 7(a)). The mesh in this scheme becomes denser and denser from the bottom to the top of the model. In the horizontal direction, the size of the elements gradually decreases from the left and right side to the middle part of the model. Specially, the area at the edge of the footing is occupied by the densest elements to ease the computational inaccuracy due to the stress concentration in this area. In the following analysis, it will be shown that this mesh scheme is refined enough to obtain an accuracy result for deterministic analysis of bearing capacity. For the probabilistic analysis, this mesh scheme is further justified in Section 4.2. For boundary conditions, horizontal movements on the vertical boundary are constrained and the nodes at the bottom are fixed in all directions. A rough strip footing is simulated by setting the horizontal velocity of the nodes representing the footing to zero.

To evaluate the bearing capacity, a downward velocity of $1.5*10^{-5}$ m/step is applied to the surface nodes on the base of the footing. The possible rotation of footing which can be induced from spatial variability of soil properties is not considered herein for simplicity. A steady state of plastic flow will develop in the soil as the step increases. The averaged unbalanced force on the interface of footing and soil at the plastic steady state is taken as the bearing capacity of the strip footing. Note that the applied velocity has an influence zone beyond the footing area. In other words, there is a velocity singularity at the ends of the footing (see the velocity field at the plastic steady state in Fig. 8(a)). This singularity is spread over the element adjacent to the footing. It is assumed that the

velocity jump (i.e. change of velocity direction from downward to upward) occurs half a zone width from the end of the footing. This assumption has little effect on the accuracy of the bearing capacity calculation as the mesh is very dense at the edge of the footing (Itasca, 2009). Hence, the averaged unbalanced force is obtained by dividing the sum of vertical footing nodal stresses by the area of the footing with its width extending to the center of the first element outside the footing (Cho and Park, 2010).

Two sets of parameters are adopted to study the effect of trend of s_u on the reliability of strip footing. For the considered two cases, namely s_u constant with depth and s_u linearly increasing with depth, the elastic modulus of 20 MPa and Poisson's ratio of 0.499 remain the same. The difference between the two cases is that for the case of s_u constant with depth, the clay soil is homogeneous with a constant s_u of 86.2 kPa (i.e. vertical dot dash line in Fig. 5(c)), and for the case of s_u linearly increasing with depth, the clay is heterogeneous with s_u linearly increasing from 40 kPa at the top to 132.4 kPa at the bottom (i.e. the solid straight line in Fig. 5(c)). Using this method, the two cases have the same mean value of s_u in the mid-depth of 3 m, which may be useful for comparison.

Fig. 8 shows the velocity vector and contours of maximum shear strain rate at the plastic steady state for s_u constant with depth and linearly increasing with depth. The failure modes in both cases are general shear failure with a well-defined wedge-shaped zone remaining elastic below the center of the footing. For the case of s_u constant with depth, the bearing capacity obtained from numerical simulation is 468 kPa, which is slightly larger than the Prandtl solution of $5.14s_u=443$ kPa (Whitlow, 1990). As expected, the rough footing has a slightly higher bearing capacity than that for a smooth footing. To further verify the bearing capacity result of footing on weighted soil, a strip footing case in Massih and Soubra (2007) is also analyzed. In this case, a rough rigid strip footing is subjected to a vertical loading. A conventional elastic-perfectly plastic model based on the Mohr–Coulomb failure criterion is used to represent the soil. The dilation angle of the soil is assumed to be equal to the friction angle(ϕ). The calculated N_c and N_γ value for a $\phi=30^\circ$ soil is $N_c=33.0$ and $N_\gamma=20.18$, respectively, where N_c and N_γ are dimensionless factors to express the bearing capacity, q_f, for an infinite strip footing under no surcharge loadings (see Eq. (14)). This result is consistent with the value calculated by Massih and Soubra (2007), i.e. $N_c=34.0$, and $N_\gamma=19.28$. The result also coincides with the analysis conducted by other researchers which are listed in Massih and Soubra (2007).

$$q_f = c^*N_c + 0.5^*B^*\gamma^*N_\gamma \tag{14}$$

where c is the cohesion of soils; B is the width of the footing; γ is the unit weight of soil.

For s_u linearly increasing with depth, the bearing capacity of strip footing, 275 kPa, is smaller than that for s_u constant with depth. The failure zone becomes small in comparison with s_u constant with depth because the s_u in shallow area ($z<3$ m) for the case of s_u linearly increasing with depth is significantly lower than that for the case of s_u constant with depth. It is worth noting that no analytical solutions exist for the bearing capacity of strip footings founded on clay soil with linearly increasing s_u. Hence, a similar case of shallow foundation taken from Zhalehjoo et al. (2012) is reanalyzed to further verify the results for linearly increasing s_u. In this case, s_u linearly increases from 25 kPa at the ground surface with an increasing rate of 10 kPa/m. The obtained bearing capacity is 149 kPa, which is almost the same as 150 kPa as reported in Zhalehjoo et al. (2012). Therefore, the adopted method to calculate the bearing capacity for linearly increasing s_u is reasonable.

4.2. Probabilistic analysis

In this section, Monte Carlo simulations are carried out to evaluate the mean of the bearing capacity (μ_{qu}), standard deviation of the bearing capacity (σ_{qu}) and probability of failure of the strip footing. Random field of undrained shear strength is first discretized using the KL expansion. Thereafter, a series of numerical simulations are performed using the Flac3d software based on the discretized random field. A FISH (the built-in programming language of Flac3d) function is adopted to assign different values of undrained shear strength to different finite difference elements.

As discussed in Section 2.3, the undrained shear strength is treated as a random field parameter and the unit weight is treated as a random variable. The elastic modulus and Poisson's ratio is assumed to be deterministic since the bearing capacity is not sensitive to these parameters. For the case of s_u linearly increasing with depth, the parameters corresponding to the linear-trend line in Fig. 5(c) (the solid straight line) are adopted, i.e. $\mu_{\gamma'}=11$ kN/m^3, $b=40$ kPa, $\mu_a=1.4$. These values are reasonable since the trend line is derived from the well developed empirical formula, namely Eq. (1). Moreover, $\mathrm{COV}_{\gamma'}$ and COV_a are set to 0.1 and 0.5, respectively. Applying Eq. (10), the statistics (mean, COV) of s_u at $z=3$ m and $z=6$ m are obtained as (86.2 kPa, 0.28) and (132.4 kPa, 0.36), respectively. As can be seen from Eq. (10), the COV of s_u increases with depth. Thus, the maximum COV of s_u is 0.36 at the bottom of the model shown in Fig. 7. It falls within the typical range [0.06, 0.8] as reported in Phoon and Kulhawy (1999). These results indicate that the selected value of COV_a is reasonable. As for the correlation length, Wu et al. (2012) pointed out that the autocorrelation length of a is conceptually the same as that of s_u. Following El-Ramly et al. (2003), the ranges of horizontal and vertical autocorrelation length of s_u are 10–40 m and 1–3 m, respectively. Hence, the horizontal and vertical autocorrelation lengths of a are set as $l_x=5$, 10, 20, 30 m, and $l_z=1$, 2, 5, 10 m. To reflect the effect of geometric parameter of strip footing, the correlation length is normalized into a dimensionless form $\Delta=l/B$ in which l is the correlation length and B is the width of strip footing. Hence, the normalized horizontal correlation length $\Delta_x=2.5$, 5, 10, 15, and normalized vertical correlation length, $\Delta_z=0.5$, 1, 2.5, 5.

4.2.1. Realization number for the Monte Carlo simulation

It should be noted that the accuracy of the reliability analysis highly depends on the number of Monte Carlo realizations. One method to determine a proper realization number is to conduct a parameter study (e.g. Cho and Park, 2010). Generally, the statistics of FS fluctuate with the Monte Carlo realization number. The fluctuation decreases as the realization number increases. A proper N can be obtained when the statistics of FS achieve a steady level. Hence, various numbers of simulations are carried out for incrementally number of simulations till no significant change in COV is observed. As $\Delta_x=2.5$, and $\Delta_z=0.5$, the mean and standard deviation of undrained bearing capacity, i.e. (μ_{qu}, σ_{qu}), for 500 and 1000 realizations of Monte Carlo simulation are (272.2 kPa, 18.3 kPa) and (272.3 kPa, 18.9 kPa), respectively. The difference seems insignificant. It can be expected that a further increase in the number of simulations will not significantly increase the accuracy of the results. Therefore, 500 Monte Carlo simulations are adopted for estimating the statistics of the bearing capacity in this study.

4.2.2. Evaluation the effectiveness of the mesh scheme

Before conducting the probabilistic analysis, it is essential to evaluate the effectiveness of the mesh scheme adopted for reliability analysis considering spatial variability of shear strength. As concluded by Ching and Phoon, 2013b, the tolerable maximum element size to achieve acceptable accuracy for soil shear strength in random field finite element analysis is surprisingly small. The satisfactory element size is governed by the line averaging effect along the potential slip surface. Hence, the mesh scheme adopted in Fig. 7(a) is justified herein.

It is well acknowledged that the performance of the strip footing highly depends on the properties of soils in influence zone (Sivakumar Babu et al, 2006). The influence zone refers to the area which the failure surface runs across. For the problems studied herein, the failure surface of bearing capacity can be approximately obtained from the contour of shear strain rate for deterministic analysis in Fig. 8. For constant s_u, the width and height of the Flac3d elements in influence zone span from 0.08 m to 0.13 m and from 0.17 m to 0.32 m, respectively (see Fig. 8(b)). For linearly increasing s_u, the width of the Flac3d elements in influence zone ranges from 0.08 m to 0.18 m while the height ranges from 0.17 m to 0.30 m (see Fig. 8(c)). These ranges can be compared with the minimum scale of fluctuation (SOF) adopted in the probabilistic analysis. As mentioned previously, the minimum horizontal and vertical correlation length adopted are 5 m and 1 m, respectively. The autocorrelation function is a commonly used squared exponential function. Based on the relation between scale of fluctuation and correlation distance, the minimum horizontal scale of fluctuation, δ_{xmin}, can be simply calculated, i.e. $\delta_{xmin}=(\pi^*\text{minimum horizontal correlation length}^2)^{0.5}=(\pi^*5^2)^{0.5}=8.86$ m. The resulting value is significantly larger than the width of elements in influence zone, i.e. 0.08 m to 0.18 m. Similarly, the minimum vertical scale of fluctuation, $\delta_{zmin}=(\pi^*\text{minimum vertical correlation length}^2)^{0.5}=(\pi^*1^2)^{0.5}=1.77$ m, is *five* times as large as of the maximum height (i.e. 0.32 m) of element in influence zone. In other words, the δ_x/(element width) $>8.86/0.18=49.2$, while δ_z/(element height) $>1.77/0.32=5.5$. On this basis, the effect of element size on mobilized strength of the spatially variable soil can be evaluated using the results of Ching and Phoon (2013b). Herein the mobilized strength refers to the yield stress recorded before the calculation fails to converge. Since the random field is generated using a midpoint strategy (rather than the element level averaging strategy) and the adopted autocorrelation model is the squared exponential function, the results of Figs. 15 and 16 in Ching and Phoon (2013b) are thus adopted for evaluation. It is worth noting that the stress state for a footing resting on layered soils is typically compressive. Hence the underlying probabilistic analyses correspond to the top two plots entitled CI and CA in Figs. 15 and 16, where CI and CA denote "Compressive stress state-Isotropic random field" and "Compressive stress state-Anisotropic random field", respectively. As shown in the top two plots in Figs. 15 and 16 in Ching and Phoon (2013b), both the sampled mean and standard deviation of the mobilized shear strength for SOF >1 m reach a steady value as δ_z/element size >5.5. Hence, the mesh scheme adopted is reasonable from the point view of mobilized shear strength.

To further evaluate the effectiveness of the mesh scheme in Fig. 7(a), a more refined mesh scheme is also adopted for the probabilistic analysis (see Fig. 7(b)). The probabilistic analysis results for the two schemes are compared. The case of $\Delta_x=2.5$, and $\Delta_z=0.5$ is taken for example. The calculated mean and standard deviation of bearing capacity, (μ_{qu}, σ_{qu}), for the relatively coarse and refined mesh schemes are, (272.2 kPa, 18.3 kPa) and (271.7 kPa, 18.6 kPa), respectively. The difference between the two results seems minor. Hence, the mesh scheme in Fig. 7(a) is effective for the bearing capacity problem considered.

4.2.3. Result of the probabilistic analysis

Fig. 9 shows one typical realization of non-stationary random field of s_u ($\Delta_x=5$, $\Delta_z=0.5$) and the corresponding velocity vector and maximum shear strain rate at plastic steady state. In Fig. 9(a), the light colors represent the low values of s_u while the dark colors represent the high values of s_u. As can be seen from Fig. 9(b) and (c), a non-symmetric failure mechanism caused by the spatial heterogeneity occurs. Such a finding cannot be manifested in the deterministic analysis or a probabilistic analysis using a single random variable model of s_u. In addition, the failure path passes through the weak zone (see Fig.9(a and c)). These results further demonstrate the validity of the proposed method for analyzing the bearing capacity of strip footing considering spatially variable undrained shear strength.

Fig. 10(a) shows the typical load–settlement curves for the first 200 realizations of non-stationary random field for $\Delta_x=5$ and $\Delta_z=0.5$. As expected, the load–settlement curves exhibit large scatter when the spatial variability of s_u is considered. The histogram of bearing capacity obtained from 500 realizations of the non-stationary random field is plotted in Fig. 10(b). The probability density function (PDF) curve of bearing capacity fitted with a Johnson distribution is also plotted in Fig. 10(b). It can be seen that the Johnson distribution can fit the histogram well. Moreover, a Kolmogorov–Smirnov (KS)

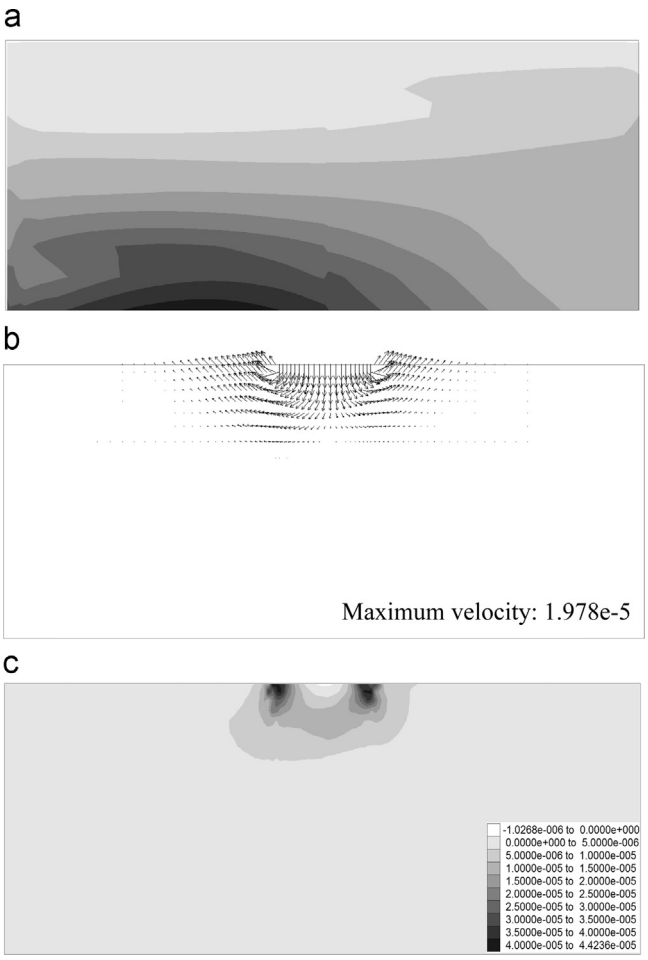

Fig. 9. Typical realization of non-stationary random field of s_u and the corresponding velocity vector and maximum shear strain rate at plastic steady state as $\Delta_x=5$, $\Delta_z=0.5$. (a) Typical realization of non-stationary random field of s_u, (b) Velocity vector for non-stationary random field of s_u, (c) Maximum shear strain rate for non-stationary random field of s_u.

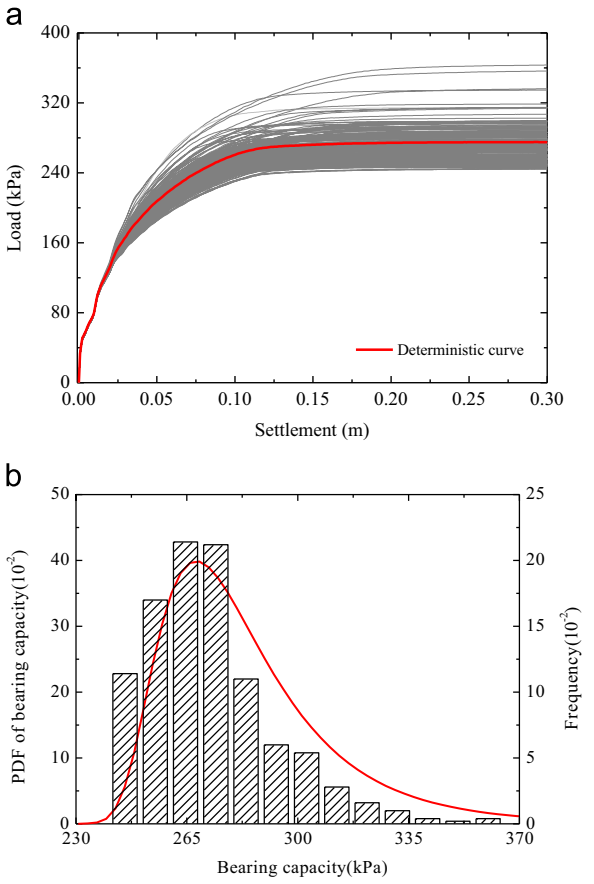

Fig. 10. Load–settlement curves and the frequency histogram of bearing capacity for non-stationary random field of s_u as $\Delta_x=5$ and $\Delta_z=0.5$. (a) Load-settlement curves for 200 realizations, (b) Frequency histogram of bearing capacity for 500 realizations.

test is conducted to investigate the fitness of the Johnson distribution. The p-value associated with the KS test is 0.306, which is larger than 0.05. Hence, there is no evidence to reject the null hypothesis that the bearing capacity is Johnson distributed. Note that some effort is also made to test whether the bearing capacity for non-stationary s_u obeys other traditional distributions, such as lognormal distribution and beta distribution. Unfortunately, all the distributions are rejected at a 5% level of significance. Therefore, the Johnson distribution is adopted to fit the distribution of bearing capacity in the subsequent analyses. Details of the parameter estimation for Johnson distribution can be found in Phoon and Ching (2013).

Fig. 11 shows the mean and standard deviation of bearing capacity for non-stationary random field of s_u and various autocorrelation lengths. Note that the mean and standard deviation of the bearing capacity are directly estimated from the results of 500 simulations. For the purpose of better clarity, the statistics of bearing capacity are normalized using the s_u value in the mid-depth of the model (i.e. $s_{u,z=3\text{ m}}=86.2$ kPa). As shown in Fig.11, the mean of the bearing capacity for s_u linearly increasing with depth is smaller than $q_{u,\text{det}}/s_{u,z=3\text{ m}}=275$ kPa/86.2 kPa=3.19, as obtained from the deterministic analysis (see Fig. 10(a)). Both the mean and standard deviation of the bearing capacity increase with increasing autocorrelation length. The change in the standard deviation of the bearing capacity with autocorrelation length is significantly larger than that in the mean of the bearing capacity. The standard deviation of the bearing capacity increasing with autocorrelation length may be attributed to the following reasons. As the autocorrelation length becomes small, the autocorrelation between the undrained shear strengths in different locations becomes weak, which induces significant fluctuation in the undrained shear strength. Thus, the continuous weak zone with low values of s_u or continuous strong zone with high values of s_u is less likely to occur. In addition, high property values at some points are more likely to be balanced by low values at the other points. All these factors reduce the variation of bearing capacity. On the contrary, a larger autocorrelation length results in a strong correlation between the undrained shear strengths at different locations. Both the continuous weak zone and continuous strong zone are more likely to occur. The variation in the bearing capacity will be large. By comparing Fig. 11(a) and (b), the statistics of bearing capacity are more sensitive to the vertical autocorrelation length than the horizontal autocorrelation length.

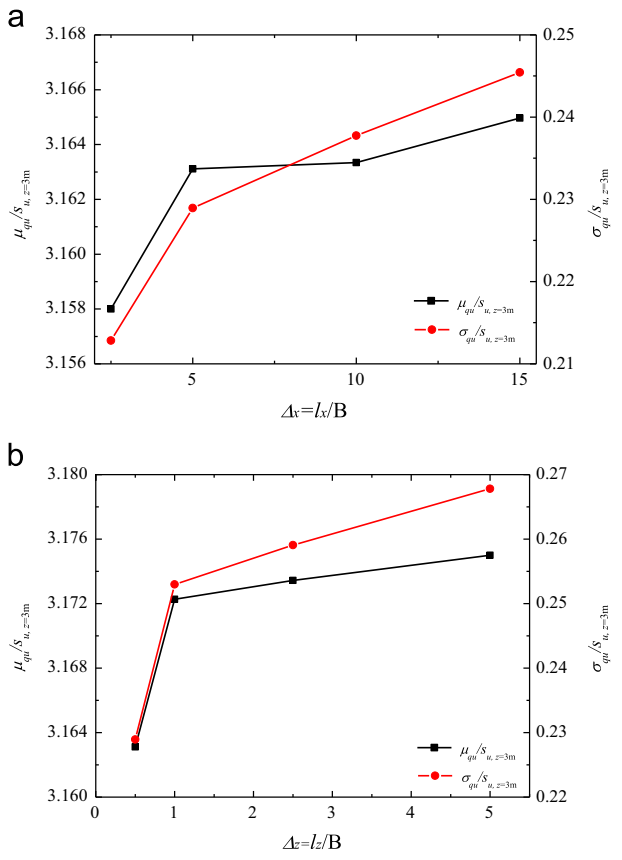

Fig. 11. The mean and standard deviation of bearing capacity for non-stationary random field of s_u and various autocorrelation lengths. (a) μ_{qu} and σ_{qu} for various horizontal autocorrelation lengths as Δ_z=0.5, (b) μ_{qu} and σ_{qu} for various vertical autocorrelation lengths as Δ_x=5.

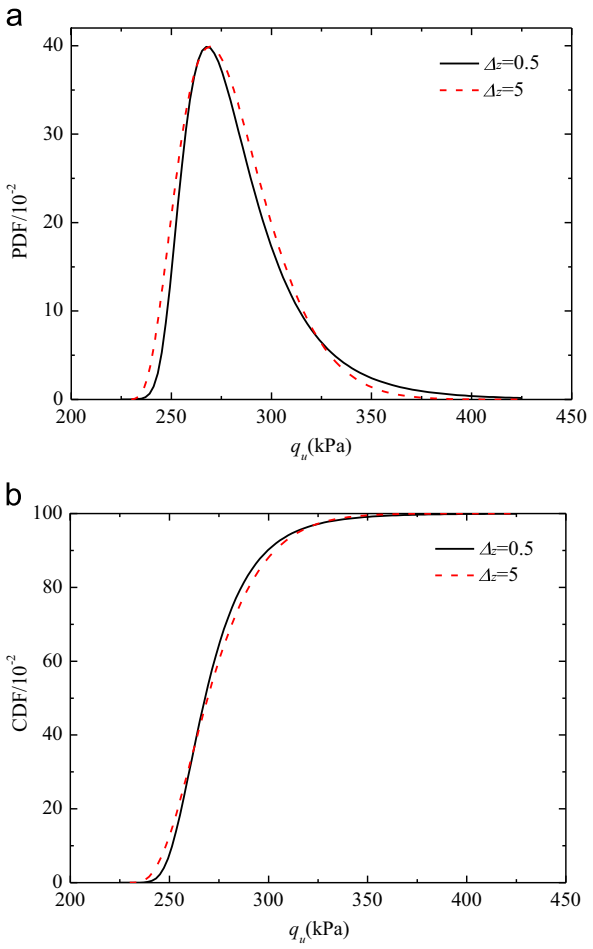

Fig. 12. CDF curves of bearing capacity for non-stationary random field of s_u as Δ_z=0.5. (a) PDF curve (b) CDF curve.

Fig. 12 plots the probability distribution function (PDF) and cumulative distribution function (CDF) for two cases with different vertical correlation distances. The PDF and CDF curves are calculated from the fitted Johnson distributions. As shown in Fig. 12, the PDF curve for small correlation distance is narrower than that for large correlation distance; the CDF curve for small correlation distance is steeper than that for large correlation distance. These phenomena can be expected because the standard deviation of q_u increases with increasing correlation distance.

In order to compare with the often-used stationary random field of s_u, the μ_{su} and σ_{su} for the stationary random field are assumed to be the same as those in the mid-depth (z=3) for the non-stationary random field. The other parameters are the same as those for the non-stationary random field. When applying a similar method, Fig. 13 shows the μ_{su} and σ_{su} for the stationary random field of s_u and Δ_z=0.5. The same observation as that shown in Fig. 11(a) for the non-stationary random field can be obtained. Compared with the results in Fig. 11(a), the increase of μ_{su} and σ_{su} with increasing vertical autocorrelation length becomes more significant.

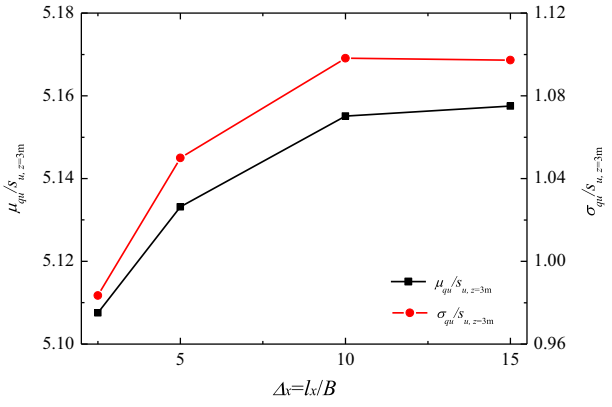

Fig. 13. The mean and standard deviation of bearing capacity for stationary random field of s_u and various horizontal autocorrelation lengths as Δ_z=0.5.

Fig. 14 compares the PDF and CDF curves of bearing capacity for two different random field models of s_u as Δ_x=5 and Δ_z=0.5. It can be seen from Fig. 14(a) that the PDF curve for the non-stationary random field is much narrower than that for the stationary random field, which indicates that the variation of bearing capacity for the non-stationary random field is significantly smaller than that for the stationary random field. This may be attributed to the following two reasons. First, as can be seen from Fig. 8(b) and (c), the possible failure path passes through the shallow area (i.e. $z<1.7$ m=0.85B)

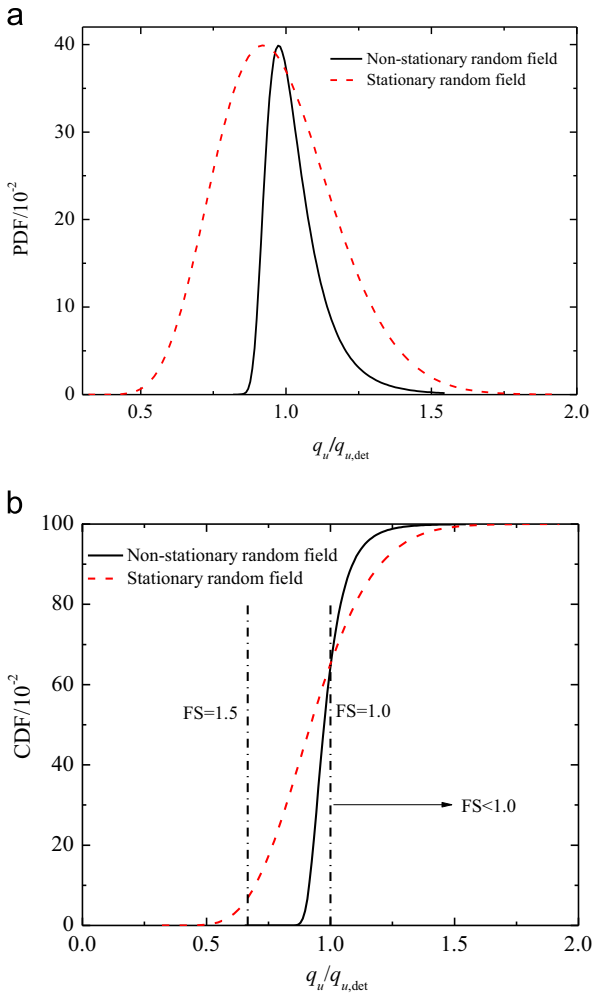

Fig. 14. Comparison of PDF and CDF curves for different random field model of s_u as $COV_a=0.5$, $COV_\gamma=0.1$, $\Delta_x=5$ and $\Delta_z=0.5$. (a) PDF of bearing capacity, (b) CDF of bearing capacity.

of the soil mass. The variation of s_u in the shallow area (i.e. $z<1.7$ m$=0.85$B) has a greater influence on the bearing capacity in comparison with the deep area (i.e. $z>1.7$ m$=0.85$B). Furthermore, the variation of s_u in the shallow area (i.e. $z<1.7$ m$=0.85$B) for the non-stationary random field is smaller than that for the stationary random field. This leads to a small variation of bearing capacity associated with the non-stationary random field. Second, it can be seen from Fig. 8(b) and (c) that the possible failure path for s_u linearly increasing with depth (i.e. $z<1.4$ m$=0.7$B) is shallower than that for s_u constant with depth (i.e. $z<1.7$ m$=0.85$B), which implies that the variation of bearing capacity for the non-stationary random field highly depends on the variation of s_u in the shallow area. This further leads to a low variability in the bearing capacity for the non-stationary random field.

In Fig. 14(b), the probability of failure for the stationary random field is significantly higher than that for the non-stationary random field. For example, as the factor of safety (FS) in deterministic analysis is 1.5 (i.e. deterministic bearing capacity, $q_{u,\mathrm{det}}=1.5$*vertical load), the probability of failure for the stationary random field, namely the probability of $q_u>$ vertical load, is 6.29%. However, for the non-stationary random field, the probability of failure at the same FS level (i.e. FS$=1.5$) is less than 1e-9. These results indicate that the often-used stationary random field model of s_u will highly overestimate the probability of failure, which may result in a conservative design of shallow foundations. On the other hand, to achieve a prescribed reliability, the requiring FS for linearly increasing s_u maybe significantly lower than that for stationary s_u. For the case of 2 m width strip footing with $\Delta_x=5$ and $\Delta_z=0.5$, a FS$=1.5$ ensures a satisfactory reliability of 5.0 (i.e. probability of failure$=\Phi(-5)=0.0000003$, where $\Phi(\cdot)=$cumulative distribution function for standard normal distribution). This level of reliability certainly meets the design requirements. However, a FS$=3$ is always required in shallow foundation designs, which might be uneconomical. Hence, it can be concluded that, the second-order non-stationary, namely the non-stationary in the standard deviation of s_u, is very important to achieve a realistic evaluation of reliability of shallow foundations. The statistics of s_u should be examined carefully so that a realistic random field model can be selected for characterizing the spatial variability of s_u. A constant COV for non-stationary spatial variability of s_u may produce misleading reliability results.

5. Conclusions

This paper has investigated the effect of spatially variable undrained shear strength that linearly increases with depth on reliability of a strip footing. Monte Carlo simulations are carried out to evaluate the statistics of bearing capacity and reliability of strip footing. They are compared with the results for the stationary random field of undrained shear strength. The following conclusions can be drawn:

1) OCR data from different sites are collected and undrained shear strength profiles are derived from these OCR data. The results show that the linear trend of undrained shear strength increasing with depth is very common for overconsolidated clays.
2) The statistics of the bearing capacity of strip footing are considerably influenced by the trend of the undrained shear strength linearly increase with depth. The mean of the bearing capacity for spatially variable undrained shear strength is smaller than that obtained from the deterministic analysis. Both the mean and the standard deviation of the bearing capacity increase with increasing autocorrelation length. The statistics of the bearing capacity are more sensitive to the vertical autocorrelation length.
3) Compared with the non-stationary random field of undrained shear strength, the stationary random field will greatly overestimate the variations in the bearing capacity. When the same factor of safety is used for the design of strip footing, the often-used stationary random field highly overestimates the probability of failure of strip footings. For

example, for a 2 m width strip footing with a FS = 1.5 and l_x = 10 m, l_z = 1 m, the failure of probability for a stationary random field (6.29%) is several orders of magnitude higher than that for a non-stationary random field ($< 1e-9$). Using the stationary random field model may be very conservative for the design of strip footings.

Acknowledgments

This work was supported by the National Science Fund for Distinguished Young Scholars (Project no. 51225903), the National Natural Science Foundation of China (Project nos. 51329901, 51409196), and the Natural Science Foundation of Hubei Province of China (Project no. 2014CFA001).

References

Asaoka, A., A-Grivas, D., 1982. Spatial variability of the undrained strength of clays. J. Geotech. Eng. Div. ASCE 108 (5), 743–756.

Cao, Z., Wang, Y., 2014. Bayesian model comparison and characterization of undrained shear strength. J. Geotech. Geoenviron. Eng. 140 (6), 04014018.

Chen, B.S., Mayne, P.W., 1994. Profiling the Overconsolidation Ratio of Clays by Piezocone Tests. Report no. GIT-CEEGEO-94-1. Georgia Tech Research Corporation & Georgia Institute of Technology, School of Civil and Environmental Engineering.

Ching, J., Phoon, K.K., 2013a. Probability distribution for mobilised shear strengths of spatially variable soils under uniform stress states. Georisk 7 (3), 209–224.

Ching, J., Phoon, K.K., 2013b. Effect of element sizes in random field finite element simulations of soil shear strength. Comput. Struct. 126, 120–134.

Cho, S.E., Park, H.C., 2010. Effect of spatial variability of cross-correlated soil properties on bearing capacity of strip footing. Int. J. Numer. Anal. Methods Geomech. 34 (1), 1–26.

Collins, B.D., Znidarcic, D., 2004. Stability analyses of rainfall induced landslides. J. Geotech. Geoenviron. Eng. 130 (4), 362–372.

El-Ramly, H., Morgenstern, N.R., Cruden, D.M., 2003. Probabilistic stability analysis of a tailings dyke on presheared clay-shale. Can. Geotech. J. 40 (1), 192–208.

Fenton, G.A., Griffiths, D.V., Zhang, X., 2008. Load and resistance factor design of shallow foundations against bearing failure. Can. Geotech. J. 45 (11), 1556–1571.

Griffiths, D.V., Fenton, G.A., Manoharan, N., 2006. Undrained bearing capacity of two-strip footings on spatially random soil. Int. J. Geomech. 6 (6), 421–427.

Griffiths, D.V., Huang, J.S., Fenton, G.A., 2011. Probabilistic infinite slope analysis. Comput. Geotech. 38 (4), 577–584.

Haldar, S., Sivakumar Babu, G.L., 2009. Design of laterally loaded piles in clays based on cone penetration test data: a reliability-based approach. Geotechnique 59 (7), 593–607.

Itasca, 2009. FLAC3D, Fast Lagrangian Analysis of Continua in 3 Dimensions. Online Manual.

Jiang, S.H., Li, D.Q., Zhang, L.M., Zhou, C.B., 2014. Slope reliability analysis considering spatially variable shear strength parameters using a non-intrusive stochastic finite element method. Eng. Geol. 168, 120–128.

Jiang, S.H., Li, D.Q., Cao, Z.J., Zhou, C.B., Phoon, K.K., 2015. Efficient system reliability analysis of slope stability in spatially variable soils using Monte Carlo simulation. J. Geotech. Geoenviron. Eng. 141 (2), 04014096.

Kasama, K., Whittle, A.J., Zen, K., 2012. Effect of spatial variability on the bearing capacity of cement-treated ground. Soils Found. 52 (4), 600–619.

Kulatilake, P.H.S.W., Um, J.G., 2003. Spatial variation of cone tip resistance for the clay site at Texas A & M University. Geotech. Geol. Eng. 21 (2), 149–165.

Kulhawy, F.H., Mayne, P.W., 1990. Manual on Estimating Soil Properties for Foundation Design. In: Final Report. Electric Power Research Inst., Palo Alto, CA (USA); Cornell Univ., Ithaca, NY (USA).

Lacasse, S., Nadim, F., 1996. Uncertainties in characterising soil properties. In: Proceedings of Uncertainty '96, Madison, Wisconsin, United States.

Le, T.M.H., 2014. Reliability of heterogeneous slopes with cross-correlated shear strength parameters. Georisk 8 (4), 250–257.

Li, D.Q., Chen, Y.F., Lu, W.B., Zhou, C.B., 2011. Stochastic response surface method for reliability analysis of rock slopes involving correlated non-normal variables. Comput. Geotech. 38 (1), 58–68.

Li, D.Q., Qi, X.H., Phoon, K.K., Zhang, L.M., Zhou, C.B., 2014. Effect of spatially variable shear strength parameters with linearly increasing mean trend on reliability of infinite slopes. Struct. Saf. 49, 45–55.

Li, D.Q., Jiang, S.H., Cao, Z.J., Zhou, C.B., Zhang, L.M., 2015a. A multiple response-surface method for slope reliability analysis considering spatial variability of soil properties. Eng. Geol. 187, 60–72.

Li, D.Q., Xiao, T., Cao, Z.J., Zhou, C.B., Zhang, L.M., 2015b. Enhancement of random finite element method in reliability analysis and risk assessment of soil slopes using Subset Simulation. Landslides, http://dxdoi.org/10.1007/s10346-015-0569-2.

Li, D.Q., Zhang, L., Tang, X.S., Zhou, W., Li, J.H., Zhou, C.B., Phoon, K.K., 2015c. Bivariate distribution of shear strength parameters using copulas and its impact on geotechnical system reliability. Comput. Geotech. 68, 184–195.

Lloret-Cabot, M., Fenton, G.A., Hicks, M.A., 2014. On the estimation of scale of fluctuation in geostatistics. Georisk 8 (2), 129–140.

Low, B.K., Lacasse, S., Nadim, F., 2007. Slope reliability analysis accounting for spatial variation. Georisk 1 (4), 177–189.

Lu, N., Godt, J.W., Wu, D.T., 2010. A closed-form equation for effective stress in unsaturated soil. Water Resour. Res. 46 (5), 1–14.

Lumb, P., 1966. The variability of natural soils. Can. Geotech. J. 3 (2), 74–97.

Luo, Z., Atamturktur, S., Cai, Y.Q., Juang, C.H., 2012. Simplified approach for reliability-based design against basal-heave failure in braced excavations considering spatial effect. J. Geotech. Geoenviron. Eng. 138 (4), 441–450.

Massih, D., Soubra, A., 2007. Numerical simulations for the bearing capacity of strip footings. Adv. Shallow Found., Colorado, USA, 1–10.

Phoon, K.K., Ching, J.Y., 2013. Multivariate model for soil parameters based on Johnson distributions. In: Withiam (Ed.), Geo-Congress 2013: Foundation Engineering in the Face of Uncertainty: Honoring Fred H. Kulhawy, Geotechnical Special Publication (GSP) No. 229. ASCE, California, United States.

Phoon, K.K., Huang, S.P., Quek, S.T., 2002. Implementation of Karhunen–Loeve expansion for simulation using a wavelet-Galerkin scheme. Probab. Eng. Mech. 17 (3), 293–303.

Phoon, K.K., Kulhawy, F.H., 1999. Characterization of geotechnical variability. Can. Geotech. J. 36 (4), 612–624.

Phoon, K.K., Quek, S.T., An, P., 2003. Identification of statistically homogeneous soil layers using modified Bartlett statistics. J. Geotech. Geoenviron. Eng. 129 (7), 649–659.

Popescu, R., Deodatis, G., Nobahar, A., 2005. Effects of random heterogeneity of soil properties on bearing capacity. Probab. Eng. Mech. 20 (4), 324–341.

Shibuya, S., Tanaka, H., 1996. Estimate of elastic shear modulus in holocene soil deposits. Soils Found. 36 (4), 45–55.

Sivakumar Babu, G.L., Srivastava, A., Murthy, D.S.N., 2006. Reliability analysis of the bearing capacity of a shallow foundation resting on cohesive soil. Can. Geotech. J. 43 (2), 217–223.

Soubra, A.H., Mao, N., 2012. Probabilistic analysis of obliquely loaded strip foundations. Soils Found. 52 (3), 524–538.

Srivastava, A., Sivakumar Babu, G.L., 2009. Effect of soil variability on the bearing capacity of clay and in slope stability problems. Eng. Geol. 108 (1-2), 142–152.

Tang, X.S., Li, D.Q., Rong, G., Phoon, K.K., Zhou, C.B., 2013. Impact of copula selection on geotechnical reliability under incomplete probability information. Comput. Geotech. 49, 264–278.

Tang, X.S., Li, D.Q., Zhou, C.B., Phoon, K.K., 2015. Copula-based approaches for evaluating slope reliability under incomplete probability information. Struct. Saf. 52, 90–99.

Teixeira, A., Honjo, Y., Correia, A.G., Henriques, A.A., 2012. Sensitivity analysis of vertically loaded pile reliability. Soils Found. 52 (6), 1118–1129.

van Genuchten, M.T., 1980. A closed-form equation for predicting the hydraulic conductivity of unsaturated soils. Soil Sci. Soc. Am. J. 44 (5), 892–898.

Vanmarcke, E., 2010. Random Fields: Analysis and Synthesis. Revised and Expanded New Edition. World Scientific Publishing, Beijing.

Wang, Y., Cao, Z., 2013. Expanded reliability-based design of piles in spatially variable soil using efficient Monte Carlo simulations. Soils Found. 53 (6), 820–834.

Whitlow, R., 1990. Basic soil Mechanics, fourth ed Prentice Hall, London.

Wu, S.H., Ou, C.Y., Ching, J.Y., Juang, C.H., 2012. Reliability-based design for basal heave stability of deep excavations in spatially varying soils. J. Geotech. Geoenviron. Eng. 138 (5), 594–603.

Zhalehjoo, N., Chenari, R.J., Pouya, K.R., 2012. Evaluation of bearing capacity of shallow foundations using random field theory in comparison to classic methods. In: GeoCongress 2012: State of the Art and Practice in Geotechnical Engineering, Oakland, CA, United States.

Zhu, H., Zhang, L.M., 2013. Characterizing geotechnical anisotropic spatial variations using random field theory. Can. Geotech. J. 50 (7), 723–734.

Zhu, H., Zhang, L.M., Zhang, L.L., Zhou, C.B., 2013. Two-dimensional probabilistic infiltration analysis with a spatially varying permeability function. Comput. Geotech. 48, 249–259.